Nanoscale

Accepted Manuscript

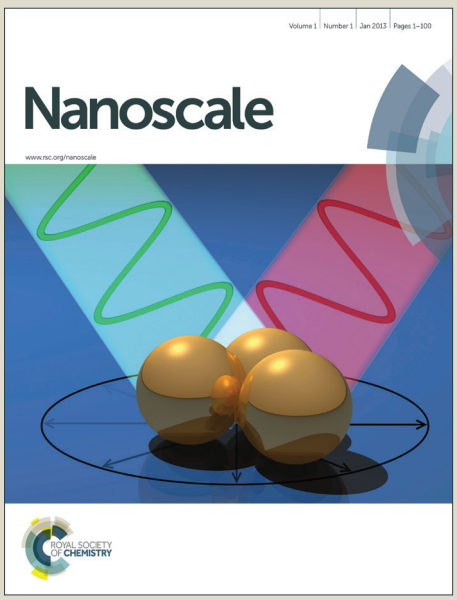

ROYAL SOCIETY OF CHEMISTRY

www.rsc.org/nanoscale

Cite this: DOI: 10.1039/c0xx00000x

www.rsc.org/nanoscale

Paper

Gd-Containing Conjugated Polymer Nanoparticles: Bimodal nanoparticles for Fluorescence and MRI Imaging

Zeina Hashim,[a] Mark Green,[a,b]* Pei Hua Chung,[a] Klaus Suhling,[a] Andrea Protti[b] , Alkystis Phinikaridou[b], Rene Botnar[b], Raha Ahmad Khanbeigi,[c] Maya Thanou,[c] Lea Ann Dailey,[c] Nicola J. Commander,[d] Caroline Rowland,[d] Jo Scott,[d] Dominic Jenner.[d]

Received (in XXX, XXX) Xth XXXXXXXXX 20XX, Accepted Xth XXXXXXXXX 20XX
DOI: 10.1039/b000000x

Aqueous bifunctional semiconductor polymer nanoparticles (SPNs), approximately 30 nm in diameter (as measured from electron microscopy), were synthesised using hydrophobic conjugated polymers, amphiphilic phospholipids and a gadolinium-containing lipid. Their fluorescence quantum yields and extinction coefficients were determined, and their MRI T_1–weighted relaxation times in water were measured. The bimodal nanoparticles were readily taken up by HeLa and murine macrophage-like J774 cells as demonstrated by confocal laser scanning microscopy, and were found to be MRI-active, generating a linear relationship between T_1 – weighted relaxation rates and gadolinium concentrations The synthesis is relatively simple, and can easily result in milligrams of materials, although we fully expect scale-up to the gram level to be easily realised.

Introduction

Interest in nanoparticles that act as multifunctional molecular imaging agents has increased in recent years[1-3]. Multimodal nanoparticles in this context refer to nanoparticles which have two or more properties which can be used simultaneously in multiple imaging techniques such as fluorescence imaging, magnetic resonance imaging (MRI), X-ray computerised tomography (CT), or positron emission tomography (PET). In any diagnosis, more than one bio-imaging technique may identify a specific problem and each imaging technique can provide complementary information. Imaging agents or probes are usually used to enable, enhance, or improve the contrast of the images obtained by these techniques, or to probe the environment[4, 5]. The use of nanoparticles as imaging probes has several advantages over conventional imaging agents. Loadability is one of the advantages where the concentration of the imaging agent can be controlled within each nanoparticle during the synthesis process. Another advantage is the tunability of the surface of the nanoparticles which can potentially extend the circulation time of the agent in the blood or target a specific location within the body[6].

Different bimodal nanoparticles which act as fluorescent probes for optical imaging and contrast agents in MRI have been reported. For the fluorescence element, either inorganic quantum dots[7, 8], fluorescent dyes[9, 10], or fluorescently labelled lipids[11] have been used. As MRI contrast agents, either superparamagnetic agents such as iron oxide (Fe_3O_4) nanoparticles[8, 12] or paramagnetic agents such as gadolinium (in the form of Gd-lipids[7] or as doping atoms[13]) have been used. Different methods of synthesis have produced various modes for incorporating multiple imaging agents. For example, one component of the system may coat the other or may be covalently attached[8], both agents may be imbedded in a host matrix such as silica[10, 14] or a polymer nanoparticle [9, 15]. Alternatively, one agent may be imbedded in a carrier which is coating the second agent[15], or both agents may be incorporated together into a micelle or liposome[11, 16]. Several articles report fluorescent and MRI active bimodal nanoparticles' properties, their synthesis and applications[1-3, 6, 15].

Conjugated polymer nanoparticles or semiconducting polymer nanospheres (SPNs) are fluorescent organic nanoparticles which are synthesised from hydrophobic conjugated polymers[17]. These nanoparticles may be used in similar applications to QDs and may even be superior to QDs due to their increased brightness and enhanced biocompatibility[18-22]. The use of conjugated polymers in bimodal systems was reported previously, where systems composed of aqueous conjugated polymers were covalently bound to gadolinium containing molecules[23, 24]. These materials however lacked the advantages of nanoparticle systems and limited the syntheses to hydrophilic conjugated polymers only.

Bifunctional (bimodal) phospholipid capped SPNs imbedded with iron oxide nanoparticles were reported previously by our group[25]. The SPNs had diameters ranging between 160 and 380 nm after centrifugation, and low quantum yields in comparison to

simple phospholipid capped SPNs[19, 25]. These bimodal iron oxide-containing SPNs compared non-favourably to similar bimodal quantum dots due to their larger diameters, lower QYs, and higher polydispersity[7]. To circumvent these problems, we report a new bimodal SPN system comprised of SPNs capped with a layer of mixed phospholipids including a diethylenetriaminepentaacetic acid-bis(stearylamide) gadolinium salt (Gd-DTPA-BSA) as the MRI-active lipid, as used previously by Mulder *et al*.[7]. The Gd-SPNs manufactured in this study showed smaller diameters and higher quantum yields than the bifunctional iron oxide SPNs previously investigated. A nanoparticle verses tissue auto-fluorescence study was also carried revealing distinguishable signals after shallow injections in euthanized animals.

Experimental Methods

Four commercially available conjugated polymers were used to form the core of the semiconducting polymeric nanoparticles: Poly[2-methoxy-5-(2-ethylhexyloxy)-1,4-phenylenevinylene] (MEH-PPV, MW 40 000 – 70 000 Da); Poly[(9,9-di-n-octylfluorenyl-2,7-diyl)-alt-(benzo[2,1,3]thiadiazol-4,8-diyl)] (F8BT, MW 5 000 – 8 000 Da); Poly[2,5-di(3',7'-dimethyloctyl)phenylene-1,4-ethynylene] (PPE, MW 4 122); Poly[(9,9-dioctyl-2,7-divinylene-fluorenylene)-alt-co-(2-methoxy-5-(2-ethyl-hexyloxy)-1,4-phenylene)] (ADS108GE, MW 111 000 Da). Three lipids were used in the outer shell of the nanoparticles:1,2-dipalmitoyl-sn-glycero-3phosphoethanolamine-N-[methoxy(polyethyleneglycol)-2000] (ammonium salt) (PEG2000-PE); 1,2-dipalmitoyl-sn-glycero-3-phosphocholine (DPPC); (diethylenetriaminepentaacetic acid)-bis(stearylamide) (gadolinium salt) (Gd-DTPA-BSA). All polymers were obtained from Sigma-Aldrich, except for ADS108GE which was obtained from American Dye Source, Inc. PEG2000-PE and DPPC were obtained from Avanti Polar Lipids, and Gd-DTPA-BSA was obtained from IQsynthesis Inc.

In a typical synthesis, 25 mg of the conjugated polymer was dissolved in 8 mL of dichloromethane (DCM). In a separate round bottom flask, 11.2 mg DPPC, 37.4 mg PEG2000-PE, and 13.9 mg Gd-DTPA-BSA were added to 25 mL of deionised water, which was covered and sonicated in a 35 kHz ultrasound water bath and maintained at a temperature below 7 °C using ice. All samples were subjected to four sonication cycles of 60 seconds each, with 30 second rest periods in between each cycle. The lipid suspension was then magnetically stirred for 1 minute followed by injection of 0.8 mL of the polymer solution over a period of 60 seconds. The flask was covered, stirred vigorously for 10 minutes, and then sonicated for 90 seconds at 7°C. Finally, the open flask was gently stirred overnight to promote full DCM evaporation. The excess lipids were removed via dialysis using Spectra/Por Float-A-Lyzer G2 MWCO 3.5 – 5 kDa cellulose ester membranes (Spectrum Laboratories, Inc.) Each membrane tube was filled with 5 mL of nanoparticle suspension and was immersed in 1 litre deionised water which was stirred and changed every 24 hours for three days. To concentrate the Gd-SPNs in water, Spectra/Por Float-A-Lyzer G2 MWCO 0.1 – 0.5 kDa cellulose ester membranes and Spectra/Gel Absorbent made of polyacylate-polyalcohol were used. The purified aqueous nanoparticle suspensions were filtered through 0.2 µm cellulose acetate filters and stored in glass vials at 4°C. PEG2000-PE was substituted by DSPE-PEG2000 (1,2-distearoyl-sn-glycero-3-phosphoethanolamine-N-[carboxy(polyethylene glycol)-2000] (ammonium salt)) to prepare the carboxylated Gd-SPNs. The carboxylated Gd-SPNs were purified in a similar manner.

Absorption spectroscopy was performed using a Hitachi U-4100 spectrophotometer and emission spectra were obtained using a Perkin Elmer LS50B luminescence spectrometer. The hydrodynamic diameters of the Gd-SPNs in water were measured using Beckman Coulter Delsa Nano C Particle Analyser (DLS). The DLS measurements were performed in quartz cuvettes prepared with at least three measurements taken for each sample. Transmission electron microscopy (TEM) was performed on an FEI Tecnai G2 F20 FE-TEM. For TEM imaging of the nanoparticles, the aqueous SPN suspensions were dropcast onto carbon coated copper grids. Nanoparticles diameters were measured using ImageJ from at least five different TEM images and 400 counts for each sample and the number distributions were plotted. A NanoSight LM10 Nanoparticle Tracking Analysis system was used to determine the hydrodynamic diameters (NTA measurements) of the Gd-SPNs. The samples were diluted before measurements, and the measurements were carried out by Ms. Agnieszka Siupa in the labs of NanoSight Ltd.

The colloidal stability of MEH-PPV Gd-SPNs in more complex media was investigated by measuring their hydrodynamic diameters in cell culture medium (CCM) and in water at 37°C, over a period of 24 hours by Malvern Zetasizer Nano ZS. 12.5 µg/mL of the nanoparticles was prepared in water or in phenol-red-free Dulbecco's Modified Eagle Medium (DMEM, obtained from Invitrogen) with 2% serum. The instrument parameters used for measurements in CCM were: Scattering angle = 173°, refractive index of particles = 1.590, refractive index of CCM = 1.337, temperature = 37°C, dynamic viscosity of CCM = 0.738x10-3 Pa s. The measurements were carried out at 10 minute intervals for the first hour, then at 2h intervals for the rest of the 24 hours. The samples were kept in the Zetasizer between measurements to maintain the same temperature throughout. The Zetasizer was set to automatically adjust its attenuations and settings before each measurement.

The quantum yields (QY) were measured by comparison with suitable fluorescent standards: Fluorescein in water (QY = 93%[26]) for F8BT and ADS108GE; Atto 390 in water (QY = 90%[27]) for PPE; Rhodamine 6G in water (QY = 95%[26]) for MEH-PPV.

The concentrations of gadolinium in the purified Gd-SPNs solutions were determined using mass spectrometry, while the concentrations of the polymer nanoparticles in water were determined by evaporating the water and dissolving the nanoparticles in $CHCl_3$ with 1% methanol. The previously obtained extinction coefficients of known concentrations of the polymers in $CHCl_3$ + 1% methanol at the wavelengths of absorption peaks (data not shown) were used in Beer-Lambert Law to determine the concentrations of the dissolved nanoparticles, and therefore determine the concentrations of the polymer nanoparticles in the aqueous nanoparticle solutions. The extinction coefficients of the aqueous Gd-SPNs solutions at the peaks of the absorption spectra were then estimated. The Beer-Lambert Law is given by

$$I = I_0 e^{-\varepsilon[c]d} \quad (1)$$

where I is the transmitted light intensity, I_0 is the incident light intensity, ε is the extinction coefficient of the sample in (mL/(mg.cm)), *[c]* is its concentration in (mg/mL), and d is the pathlength in (cm).

Live cell confocal laser scanning fluorescence microscopy of MEH-PPV Gd-SPNs was performed using the human HeLa cell line (American Type Culture Collection). HeLa cells were cultured in phenol red Dulbecco's modified eagle's medium (DMEM) supplemented with 10% fetal bovine serum (FBS), 1% non essential amino acids, 1 mM sodium-pyruvate and 0.1 % penicillin/streptomycin at 37°C and 5% CO_2. The cells were seeded in a 6-well glass bottom plate (WaferGen Smartslide-6TM micro-incubator) 24 hours prior to the addition of 20 µl MEH-PPV Gd-SPNs (initial concentration = 0.05 mg/mL). After overnight incubation, cells were washed 4-5 times with phenol red-free DMEM to remove Gd-SPNs, which were not associated with or internalised by the cells. During imaging, cells were maintained in phenol red-free DMEM at 37°C. Image acquisition was carried out using an inverted Leica TCS SP2 confocal microscope. Fluorescence excitation was stimulated by the 488 nm line of a continuous wave Ar+ laser through a 63x water immersion objective (HCX PL APO, NA = 1.2), with a line scan speed of 400 Hz. Emitted fluorescence at 570 – 650 nm was collected through the same objective, dispersed through a prism and detected using a photomultiplier. Transmitted light images were collected simultaneously. Gd-SPNs were pseudo-coloured green and images are representative of at least three separate experiments.

Fixed cell confocal laser scanning fluorescence microscopy of MEH-PPV Gd-SPNs was performed using the murine macrophage-like J774 cell line (American Type Culture Collection). J774 cells were cultured in phenol red Dulbecco's modified eagle's medium (DMEM) supplemented with 10% fetal bovine serum (FBS), 1% L-glutamine, 1% sodium-pyruvate and 1% penicillin/streptomycin at 37°C and 5% CO_2. The cells were seeded at 1x106 cells/cm^2 in 8-well glass chamber slides (LabTekTM Chamber SlidesTM) 24 hours prior to the addition of 50 µl MEH-PPV Gd-SPNs suspended in cell culture medium (initial concentration = 0.2 mg/mL). Gd-SPNs were incubated with J774 cells for two hours and were subsequently washed 4-5 times with phosphate buffered saline (PBS) pH 7.4 to remove Gd-SPNs which were not associated with or internalised by the cells. Cells were fixed with 4% paraformaldehyde in PBS and the nuclei stained 30 min under light exclusion with 4',6-diamidino-2-phenylindole (DAPI). The cells were then mounted in glycerine: PBS (1:1) and visualised using a Leica DMIR E2 confocal microscope (Leica Microsystems, Milton Keynes, UK). Fluorescent emissions from DAPI (λ_{ex} = 205 nm; λ_{em} = 430-480 nm) and Gd-SPNs (λ_{ex} = 488 nm; λ_{em} = 570-650 nm) were collected using separate channels at a magnification of 63x and at an optical plane selected at half the cell height. Instrument gain and offset values were adjusted using the negative control and remained constant for all subsequent experiments. Images obtained from each scan were pseudo-coloured blue (DAPI) and gold-red (Gd-SPNs), then overlapped afterwards to obtain a multicoloured composite image. The presented results depict a representative image from at least three experiments.

Imagestream X Mk I analysis was completed to identify intracellular Gd-SPNs after a 24 hour time period. J774A.1 cells were plated into a 24 well plate at a density of 8x105 cells/mL and incubated as previously described overnight. Cell media was removed and replaced with 1 mL fresh complete DMEM along with 20 µL of MEH-PPV Gd-SPNs. Cells were then incubated for a further 24 hrs. Cell media was removed and cells were washed once with phosphate buffered saline (PBS, Gibco, UK). Cells were harvested into 1 mL PBS and micro centrifuged at 400g for 5 mins. Cells were then resuspended in a final volume of 75 µL 1% paraformaldehyde/PBS solution. Cell samples were run on an ImageStream X Mk1 (Amnis Merckmillipore, Seattle, USA) at x40 magnification with a cell classifier of bright field area lower limit 50 µM applied to remove small debris, with a 488 laser adjusted to 25 mW. 10,000 events were collected using these setting. Data was analyzed in IDEAS software version 6.0.217.

The fluorescence lifetime of MEH-PPV Gd-SPNs was measured by time-correlated single photon counting using a Leica TCS SP2 inverted scanning confocal microscope coupled with a Becker & Hickl SPC830 card in a 3-GHz, Pentium IV, 1-GB RAM computer running Microsoft Windows XP. A pulsed diode laser (Hamamatsu PLP10) with wavelength of 470 nm, pulse duration 90 ps, and a repetition rate of 20 MHz was used as the excitation source. The emission was collected through a bandpass filter onto a cooled PMC 100-01 photomultiplier detector Becker & Hickl, a hybrid detector based on a Hamamatsu H5772P-01 photomultiplier. The fluorescence decay was then fitted by a triple exponential decay model using Becker & Hickl SPCImage software. The intensity-weighted and amplitude-weighted average fluorescence lifetimes were calculated from the multi-exponential decay.[28, 29]

Conjugation of the carboxylated Gd-SPNs with IgG was performed using a standard Sulpho-NHS and EDC method (as described by Howes *et al.*[19]). Successful conjugation was confirmed by gel filtration and fluorescence detection from washed antibody-coated plates as follows; 100 µL (Gd-SPNs)-IgG solution was added to the wells of an immunosorb assay plate. Also 100 µL unconjugated IgG was added to separate wells as a negative control. The plate was incubated overnight at 4ºC, then, washed 5 times with PBS to remove the unbound materials. Fluorescence from the washed wells was then analysed at λ_{ex} = 485 nm and λ_{em} = 536 nm. A weak Fluorescence signal was detected from the wells of the (Gd-SPNs)-IgG but not from the wells of unconjugated IgG, which means that the nanoparticles were tightly bound to the antibodies.

A simple indirect ELISA test was used to demonstrate that the bound nanoparticles to the antibodies did not adversely affect their ability to bind to their target ligands as follows; immunosorb plates were coated with diluted antigen (in carbonate buffer) by overnight incubation at 4ºC, then blocking with 1% skimmed milk PBS solution for 1 hour at room temperature. Plates were then washed in PBS and blotted dry before use. MEH-PPV (Gd-SPNs)-IgG or non-conjugated IgG were diluted in 1% skimmed milk PBS-T solution and added to the plates at a range of dilutions. The plates were incubated for 1 hour at 37 ºC then washed five times in PBS. Diluted goat anti-mouse IgG horse raddish peroxidase conjugate (obtained from AbD Serotec;

diluted 1/4000 in 1% Skimmed milk PBS) was then added to the plates and they were incubated at 37ºC for a further hour then washed in PBS. 100 µL TMB chromogen/substrate (obtained from Sigma) was added to each well in the plates, and the plates were left at room temperature for 10 minutes. The colour development was stopped with a stopper solution (also obtained from Sigma), and finally, the absorbencies of the plates' wells were detected at 450 nm within 30 minutes of stopping. The strength of the antigen-antibody reaction was determined by the intensity of the absorbance of the dye used.

For the assessment of F8BT Gd-SPNs fluorescence against animal auto-fluorescence; a rat pup was euthanized and 100 µL F8BT Gd-SPNs solution was injected subcutaneously into its scruff (initial concentration = 110 µg/mL). The rat was then imaged using an IVIS Spectrum (Caliper LS, Perkin Elmer) using a range of excitation and emission filters. The image obtained from the most optimum settings (excitation filter 465 nm and emission filter 540 nm) was then processed using the IVIS Spectrum analytical 'Image Math' tool and the background auto-fluorescence was subtracted resulting in an image detailing the fluorescence solely from the Gd-SPNs' emission.

For the assessment of the fluorescence of antibody-conjugated and unconjugated MEH-PPV Gd-SPNs against animal auto-fluorescence; cadavers from euthanized adult female Balb/c mice (Charles River, UK) were injected at three locations with either antibody-conjugated MEH PPV Gd-SPNs or unconjugated MEH-PPV Gd-SPNs as follows: 100 µL MEH-PPV (Gd-SPNs)-IgG solution (neat concentration ~ 1000x diluted Gd-SPNs with an initial concentration of ~ 35.6 µg/mL)) was injected into the quadriceps muscle, 100 µL MEH-PPV Gd-SPNs solution (concentration ~ 35.6 µg/mL) was injected subcutaneously on the ventral surface, and 100 µL MEH-PPV Gd-SPNs solution (concentration ~ 35.6 µg/mL) was injected deep into the chest cavity. The mice were then transferred to the IVIS isolator and were imaged using an IVIS Spectrum (Caliper LS, Perkin Elmer). An optimal excitation filter of 465nm and an optimal emission filter of 560nm were then used to generate composite fluorescent images.

To determine whether Gd-SPN fluorescence is affected by standard tissue histopathology processing methods, two mouse cadavers were injected with MEH-PPV Gd-SPNs into the spleen. The spleens were then aseptically removed. One spleen was placed into 4% formaldehyde fixative and the second one was placed into liquid nitrogen for snap freezing. Then both were processed for histopathology.

MRI was performed at a clinical 3T (Philips, Germany) and at a pre-clinical 7T (Agilent, Oxford UK) magnet. The sequence used at the 3T employed two non-selective inversion pulses with inversion times ranging from 20 ms to 2000 ms, followed by eight segmented readouts for eight individual images. The two imaging trains result in a set of 16 images per slice with increasing inversion times. For T_1 mapping the acquisition parameters were: FOV = 36x22x8, matrix = 192x102, in-plane resolution = 0.18x0.22mm, measured slice thickness = 0.5mm, slices = 16, TR/TE = 9.6/4.9ms, flip angle = 10°. The method used at 7T was a Look-Locker[30]. The sequence used a 180 degrees pulse to invert the magnetization of the samples.

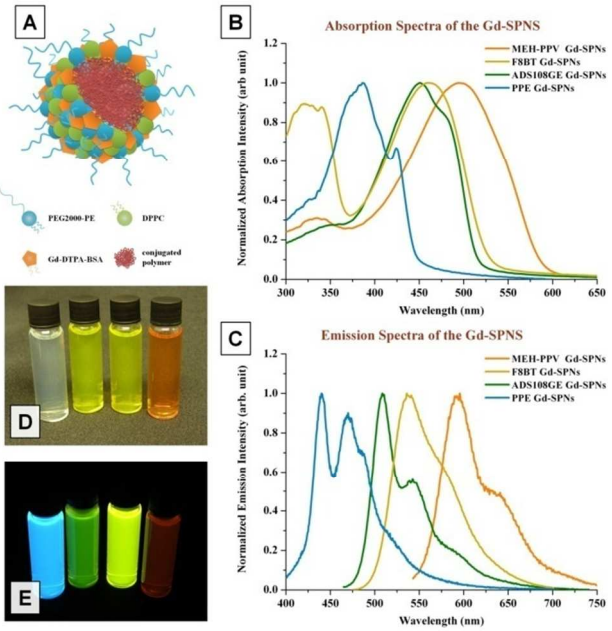

Fig. 1 (A) A schematic representing a Gd-SPN. The (B) absorption and (C) emission spectra of the four aqueous Gd-SPN solutions, and two photographs of the SPN solutions under (D) ambient light and (E) a 35 nm UV-lamp.

Table 1 A summary of the properties of the aqueous Gd-SPNs.

Property	PPE Gd-SPNs	ADS108GE Gd-SPNs	F8BT Gd-SPNs	MEH-PPV Gd-SPNs
Absorption peak (nm)	388	450	460	495
Emission peak (nm)	470 & 440	508	539	592
Quantum yield of purified Gd-SPNs (%)	22.0	7.0	33.1	1.5
Quantum yield of non-purified Gd-SPNs (%)	25.6	6.9	35.8	1.7
Quantum Yield of polymer in DCM (%)	59.2	92	68.6	15.9
Quantum Yield of reference SPNs[19]	19.0	-	26.9	1.3
Extinction coefficient ($L.g^{-1}.cm^{-1}$) at wavelength (nm)	66.0±0.3 at λ = 390	91.3±0.6 at λ = 450	41.4±0.2 at λ = 450	74.5±0.2 at λ = 490
TEM mean diameter (nm)	31.5	34.6	19.0	30.3
TEM standard deviation of diameters (nm)	21.5	17.2	7.5	18.0
DLS cumulants diameter in water (nm)	119.6	110.8	111.9	117.0
DLS poly-dispersity index	0.3	0.2	0.2	0.2
NTA (mean ± SD) (nm)	128±37	66±28	70±27	118±39
Gadolinium concentration in a non-concentrated sample (µM)	51.3	74.3	77.1	119.3

The acquisition started 10ms after the application of inversion pulse; TR = 100ms; TReff = 3700ms; 30 repetitions during the TReff; TE = 1.5 ms; FOV = 30x30mm2, 1mm thickness, matrix size = 9x96; 1 average; 1 slice; 4 phase encoding steps per pulse; scan time ~ 2min. The inversion pulse consisted of a non-selective adiabatic 180º of 8 ms while the flip angle of the turbo-FLASH imaging sequence was 20º.

The R_1 values of the samples were calculated using of ImageJ software (NIH, Bethesda, MD). The images were loaded and fit for a T_1 relaxation curve. R_1 values were consequently associated to the concentration values using Microsoft Excel. T_1 values were computed on a pixel-by-pixel basis using an in house Matlab software[31].

Results and Discussion

Colloidally stable gadolinium-containing conjugated polymer nanoparticles (Gd-SPNs) were successfully synthesised in aqueous media from the following polymers; MEH-PPV, F8BT, PPE, and ADS108GE. A schematic of the Gd-SPNs is presented in Fig. 1(A). The nanoparticles maintained the fluorescence of their constituent polymers and were found to be MRI-active and suitable for fluorescence bio-imaging. The optical properties of the Gd-SPNs are presented in Table 1. The absorption and emission spectra of the four aqueous Gd-SPNs produced in this study are presented in Fig. 1(B and C). They were found to exhibit similar spectral positions to the free polymers in organic solvents and to previously reported SPNs[18, 19, 25]. Images of Gd-SPN solutions under ambient light and UV excitation (365 nm) are shown in Fig. 1(D and E).

The brightness of the nanoparticles is important in optical cell imaging, and the brightness depends on two factors; the fluorescence quantum yield (QY) and the wavelength-dependent extinction coefficient. The brightness can be expressed as the QY multiplied by the extinction coefficient, hence the higher the two values, the greater the emission brightness. The quantum yields of the Gd-SPNs are shown in Table 1; purification reduces the QY slightly, whilst the particles exhibit notably lower QYs than the constituent polymers dissolved in DCM (also shown in Table 1). It has been noted previously[18] that the increased bending and twisting of the polymer chains in SPNs, due to the decrease in their size resulted in a decrease in their QY. The slight decrease in QY of the SPNs after purification can therefore be attributed to the removal of bulk polymer and larger particles. Furthermore, the QYs of the Gd-SPNs are comparable to the QYs of the non-gadolinium-containing SPNs prepared previously by our group[19] (also shown in Table 1) verifying that the inclusion of gadolinium in the nanoparticle synthesis process is not detrimental to the fluorescence properties in comparison to the bimodal SPNs imbedded with iron oxide nanoparticles, which suffered from a substantial quantum yield reduction[25]. Three of the four Gd-SPNs reported here also followed the trend that the higher the QY of the polymer in its free configuration in organic solution, the higher the QY in the nanoparticle form, similar to our previous observations[18].

In addition to QY, the second factor which affects brightness is the wavelength-dependent extinction coefficient. In order to calculate the extinction coefficient from Beer-Lambert's Law, the concentration of the polymer in the sample after purification and

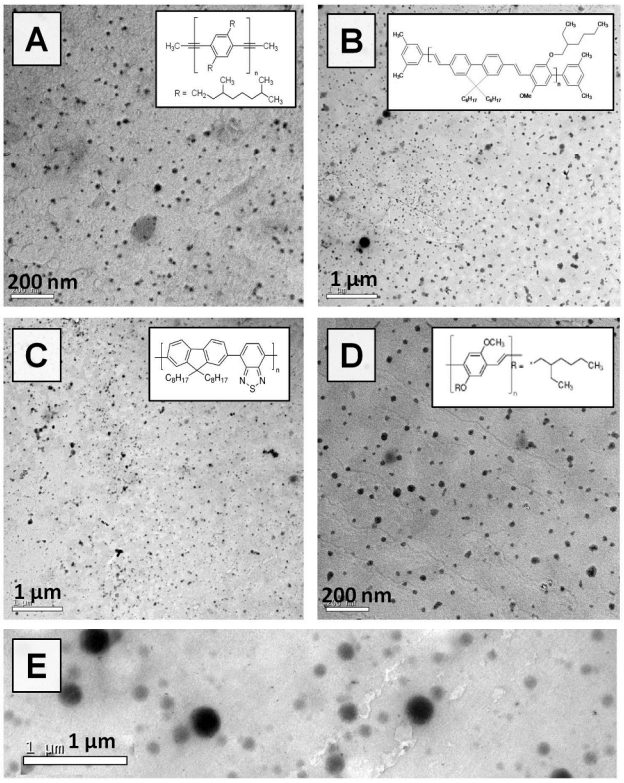

Fig. 2 TEM images of purified (A) PPE Gd-SPNs, (B) ADS108GE Gd-SPNs, (C) F8BT Gd-SPNs, (D) MEH-PPV Gd-SPNs, and non-purified (E) MEH-PPV Gd-SPNs. Bar-scales are 200 nm in (A, D), and 1 µm in (B, C, E).

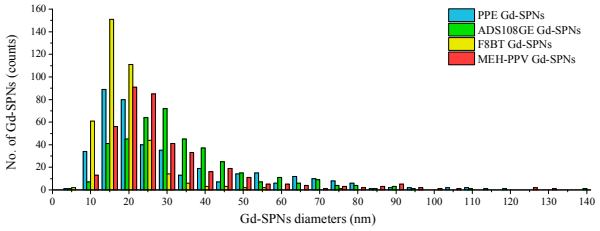

Fig. 3 Gd-SPNs number distributions measured from TEM images.

filtration was determined. Therefore, a method for determining the final polymer concentration was developed. To this end, the nanoparticles were redissolved back into an organic solvent (CHCl3 + 1% methanol) resulted in the unwinding of the polymer chain, releasing the individual polymer chains back into solution in their free forms, as confirmed by DLS. The extinction coefficients of the dissolved polymers from the Gd-SPN suspensions were calculated and are presented in Table 1. The high extinction coefficients combined with the QYs of the Gd-SPNs resulted in brightly emitting materials as observed under the UV-light in Fig. 1(E).

TEM images of the purified Gd-SPNs are presented in Fig. 2(A – D), and a TEM image of non-purified MEH-PPV Gd-SPNs prepared using double the volume of polymer solution (i.e. 1.6 mL instead of 0.8 mL) is presented in Fig. 2(E). Interestingly, the initial volume of the polymer solution was found to be one of the

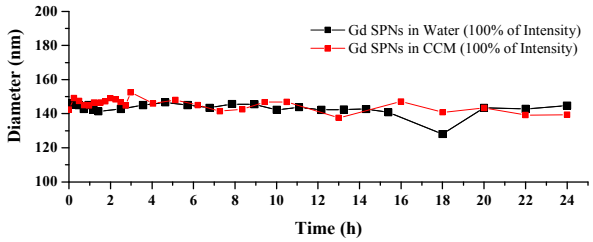

Fig. 4 Diameters of MEH-PPV Gd-SPNs, measured by DLS (cumulant results) in water and in cell culture medium (CCM) over a period of 24 hours.

crucial factors affecting the final particle diameter. Increasing the volume of polymer solution was found to produce a corresponding increase in nanoparticle diameter; the use of 1.6 mL polymer solution in the synthesis produced polymer nanoparticles with diameters of ca. 200 nm as shown in Fig. 2(E). By using the standard volume (0.8 mL) in the typical syntheses presented here, one ensured that most of the nanoparticles were below 200 nm in diameter before the purification process. During purification, 0.2 µm filters were used to remove any dust, bulk polymer, or remaining large particles. The particle size distributions of the purified Gd-SPNs as derived from the TEM images are shown in Fig. 3. For all four Gd-SPN systems, diameters varied between 6 – 140 nm, with average diameters below 35 nm and standard deviation values between 7 – 22 nm (Table 1). Table 1 also shows the average diameters of the nanoparticles in water measured using DLS (cumulant results). The randomly measured diameters using DLS for all four particle types were found to be similar (~111 – 117 nm) with low standard deviations. The average hydrodynamic diameters which also take into account the non-TEM visible lipidic shells of the Gd-SPNs, measured using NanoSight nanoparticle tracking analysis (NTA), ranged between 66 – 128 nm (also shown in Table 1). Similar to the average diameters measured from TEM, the average hydrodynamic diameters of the Gd-SPNs also had low standard deviations (27 – 39 nm). The polydispersity index (PDI) (measured by DLS, with 0 PDI being an ideally monodisperse system and 1 PDI being a highly polydisperse system) of the Gd-SPNs, also shown in Table 1, was found to be ca. 0.2. This correlated well with the low standard deviations and the TEM images where nanoparticles diameters of a few nanometres up to 140 nm were observed. The large discrepancy between particle diameter observed by TEM and DLS methods can be attributed to the thick ligand shell. The particle size has not been optimised, with various applications demanding differing sizes.

The nanoparticles were also found to be colloidally stable in more complex media. This was concluded from a study measuring the hydrodynamic diameters of similarly synthesised MEH-PPV Gd-SPNs in water and in cell culture medium (CCM) over a period of 24 hours (Fig. 4). The colloidal stability of the nanoparticles in more complex media is especially important in bio-imaging applications since aggregates may influence fluorescence properties as well as the cells interactions.

The uptake of MEH-PPV Gd-SPNs in two different cell lines was investigated using confocal laser scanning fluorescence imaging and one cell line using imaging flow cytometry

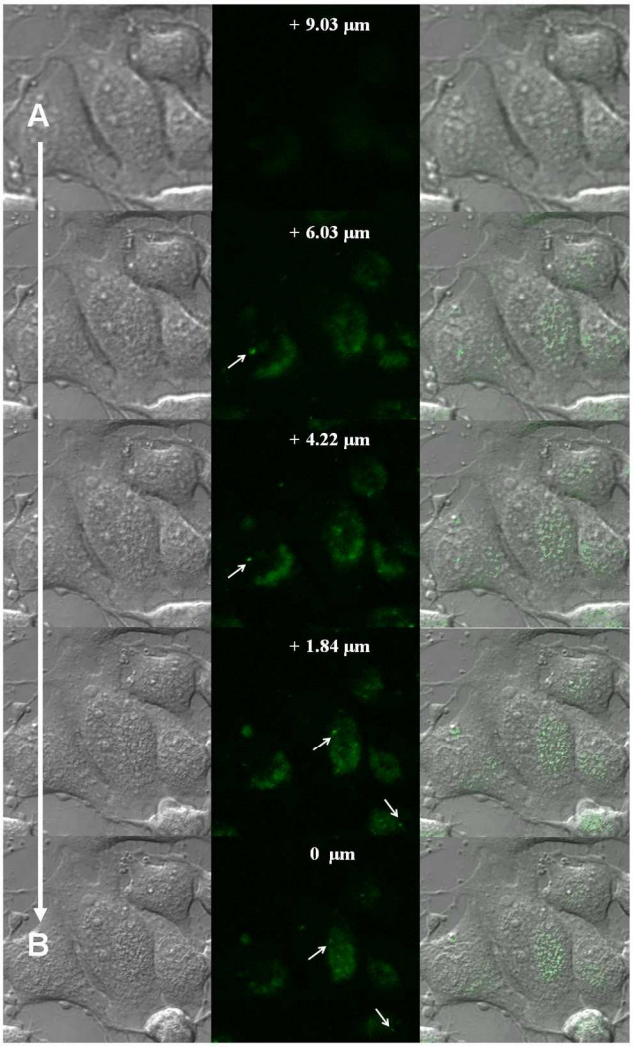

(Imagestream X): the human epithelial-like cell line, HeLa (Fig. 5), and the murine macrophage-like cell line, J774 (Fig. 6 and

Fig. 5 A cross-sectional scan of live epithelial-like HeLa cells incubated overnight with 0.05 mg/mL MEH-PPV Gd-SPNs under bright field (left column) and fluorescence excitation (middle column). The right column is an overlay of the bright field and fluorescent images. Optical sections of the cells were taken from the top (A) to the bottom (B) of the cell monolayer.

Fig. 7). As is typical for interactions between PEGylated particles approximately 100 nm in diameter and epithelial-like cells [32-35], a limited internalisation of MEH-PPV Gd-SPNs was observed in HeLa cells after overnight incubation of the particles with the cells. The diffuse green fluorescence observed in the optical sectioning of the HeLa cells in Fig. 5 is indicative of endocytic uptake of very small particles, while the brighter spots of fluorescence denoted by arrows may be indicative of the uptake of aggregated particles or vesicular fusion within the cell. In contrast, a qualitative comparison of the uptake of MEH-PPV Gd-SPNs in the macrophage-like cell line, J774, shows a much higher internalisation of particles after only two hours of incubation. This is typical of professional phagocytic cells, such as macrophages, which unlike epithelial cells, are designed to efficiently ingest large amounts of particulate matter (even when

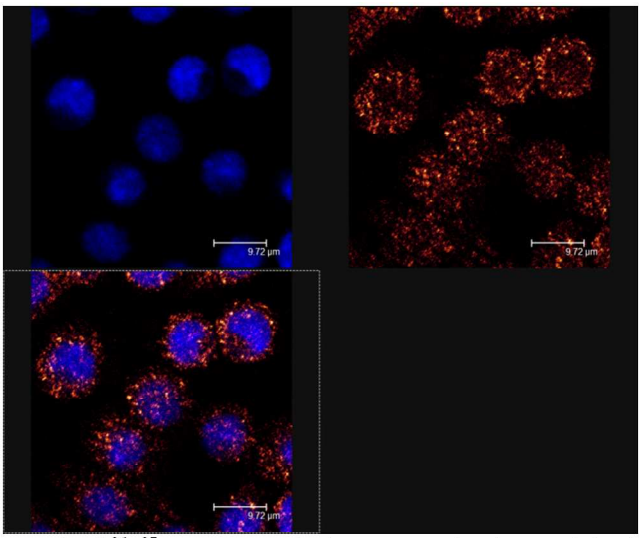

PEGylated)[36, 37]. As expected, the pattern of Gd-SPN derived fluorescence (pseudo-coloured golden-red) in the J774 cells is

Fig. 6 A cross-sectional scan of fixed J774 macrophage-like cells after a two hour incubation period with 0.2 mg/mL MEH-PPV Gd-SPNs. The top left image shows the nuclear stain fluorescence (DAPI; pseudo-coloured blue); the top right image shows fluorescence from the MEH-PPV Gd-SPN (pseudo-coloured golden-red) and the bottom left image is an overlay of the of the two. The optical plane was set at the midpoint between the top and bottom of the cell monolayer.

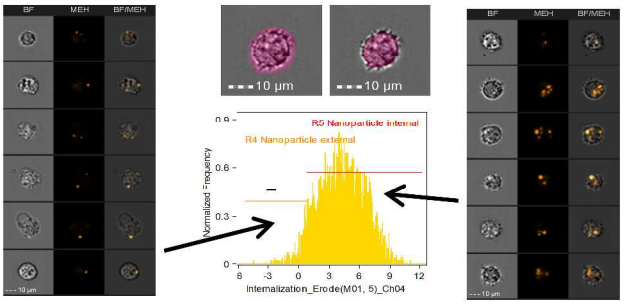

Fig. 7 Data analysis of MEH-P Gd-SPNs inside J774A.1 cells using ImageStream X. A gating strategy to identify cells with internalized MEH-PPV Gd-SPNs was used. Cell in best focused were selected first using gradient RMS feature, then single cells were gated using area vs aspect ratio, cells positive for Gd-SPNs were then selected using intensity vs max pixel. Then an internal mask was created (A = default mask B = internal mask) and the internalization feature was used to calculate the ratio of fluorescence within the internal mask as compared to the whole cell, the higher the score obtained the greater fluorescence within the internal mask and the more internalized MEH-PPV Gd-SPNs. Internalization scores were plotted on a histogram (C) and gates were drawn for the cells where MEH-PPV are membrane bound (D – 5.7%) and where MEH-PPV are truly internalized (E 94.3%).

indicative of vesicular uptake; however, in contrast to the HeLa epithelial-like cells, the fluorescence signal is much sharper, possibly indicating a greater number of particles per vesicle.

Both images in Fig. 5 and Fig. 6 demonstrate that Gd-SPNs are suitable for cellular fluorescence imaging applications in different cell types and behave similarly to other types of nanoparticles of a similar size with a PEGylated surface chemistry[38-40]. As with

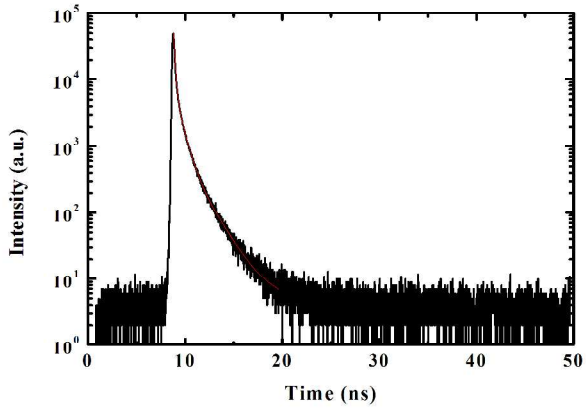

Fig. 8 The fluorescence lifetime of MEH-PPV Gd-SPNs. The decay is fitted by a three-exponential function using B&H SPCImage software.

other types of particulate imaging agents, the surface of Gd-SPNs may be modified to target specific cell types or intracellular structures. Further, Gd-SPNs are superior to a variety of fluorescent particles or small molecule fluorescent dyes due to their highly stable fluorescence with little to no photo-bleaching after multiple image acquisitions or long storage periods[21]. Imaging flow cytometry also indicated that the Gd-SPNs are suitable for internalisation and imaging applications (Fig.7). After 24 h, 94% of J774.A1 macrophages were found to have internalised the Gd-SPNs with 5.7% having membrane-associated Gd-SPNs.

Other than the fluorescence intensity, used to obtain the images described above, fluorescence lifetime, which is the average time a fluorophore maintains its excited state before emitting a photon, is another optical parameter which can be used to obtain images in fluorescence lifetime imaging microscopy (FLIM).[5, 41] The fluorescence lifetime of a fluorophore can vary according to its geometrical conformation, internal rotation and twisting, and its interactions with its surroundings such as nearby molecules[41]. Therefore, the fluorescence lifetimes of the nanoparticles prepared in this study are expected to be different from the fluorescence lifetimes of their constituent polymers. The fluorescence lifetime of MEH-PPV Gd-SPNs in solution (water) was measured to be 0.12 ns (89.4 %), 0.55 ns (9.3 %) and 1.67 ns (1.3 %) yielding an average lifetime of 180 ps (amplitude-weighted) and 429 ps (intensity-weighted) as seen Fig. 8. The increased coiling and packing of the polymer chains in the nanoparticles was expected to cause an increase in the fluorescence lifetime of the polymer. Zhang *et al*. reported the fluorescence lifetime of MEH-PPV in a good solvent was 0.35 ns (single exponential fit), and in a good/poor solvent mixture was 1.29 ns (7.2%) and 0.57 ns (92.8%)[42], yielding an average lifetime of 662 ps (intensity-weighted) for the coiled up polymer in the solvent mixture. However, the fluorescence lifetime measurements of the Gd-SPNs were found to be substantially lower than that reported for MEH-PPV in its free form. Compared to QDs (lifetimes between 10 – 30 ns and up to 500

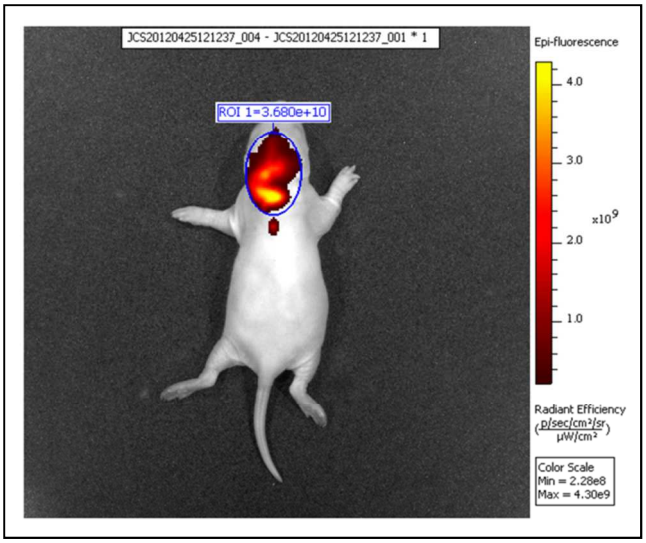

ns)[41], the fluorescence lifetime of MEH-PPV Gd-SPNs is much shorter.

Fig. 9 The fluorescence of F8BT Gd-SPNs in an euthanized rat, after subcutaneous injection and auto-fluorescence subtraction. The region of interest (ROI) shows a radiant efficiency of 3.680 x 10^{10}.

To conjugate the nanoparticles with any type of antibody, the nanoparticles must include conjugation sites (such as carboxylic groups) on their surfaces. Carboxylation can be introduced to the nanoparticle surfaces by substituting the non-carboxylated PEGylated lipid (PEG2000-PE) with a carboxylated PEGylated lipid (1,2-distearoyl-sn-glycero-3-phosphoethanolamine-N-[carboxy(polyethylene-glycol)-2000] (ammonium salt)) (DSPE-PEG2000) in the synthesis process. To this end, carboxylated MEH-PPV Gd-SPNs were synthesised and purified from excess lipids. Conjugation with IgG[43] was then performed by linking the carboxylic groups on the nanoparticles surfaces to the amine groups of the antibodies using a method described elsewhere[19]. Successful conjugation was confirmed by gel filtration and fluorescence detection from washed (Gd-SPNs)-IgG-coated plates but not from washed unconjugated-IgG-coated plates. With a simple indirect ELISA test, the bound nanoparticles were found not to affect the antibodies' ability to bind to their target ligands.

In an assessment of Gd-SPNs fluorescence against animal tissue's auto-fluorescence, 100 µL F8BT Gd-SPNs (yellow emitting; QY ~ 33%, concentration = 110 µg/mL) was injected subcutaneously into a euthanized rat's scruff, and the rat was imaged under an Elmer IVIS spectrometer. The Gd-SPNs' fluorescence was found to be visible through the rat's tissue and distinguishable from the tissue's auto-fluorescence despite being in the yellow region of the visible spectrum, as shown in Fig. 9. In a further investigation, mouse cadavers were injected at three locations with either antibody-conjugated MEH-PPV Gd-SPNs or unconjugated MEH-PPV Gd-SPNs (red emitting; QY ~ 1.5%; concentration ~ 36 µg/mL). The rationale for using MEH-PPV rather than F8BT is the preferred emission wavelength, as red emitting particles are assumed to be more useful to biologists. Firstly, 100 µL MEH-PPV (Gd-SPNs)-IgG solution (l000 x dilution of 35.6 µg/mL Gd-SPNs solution) was injected into the quadriceps muscle of a euthanized mouse. In a second injection, 100 µL of MEH-PPV Gd-SPNs (concentration ~ 35.6 µg/mL)

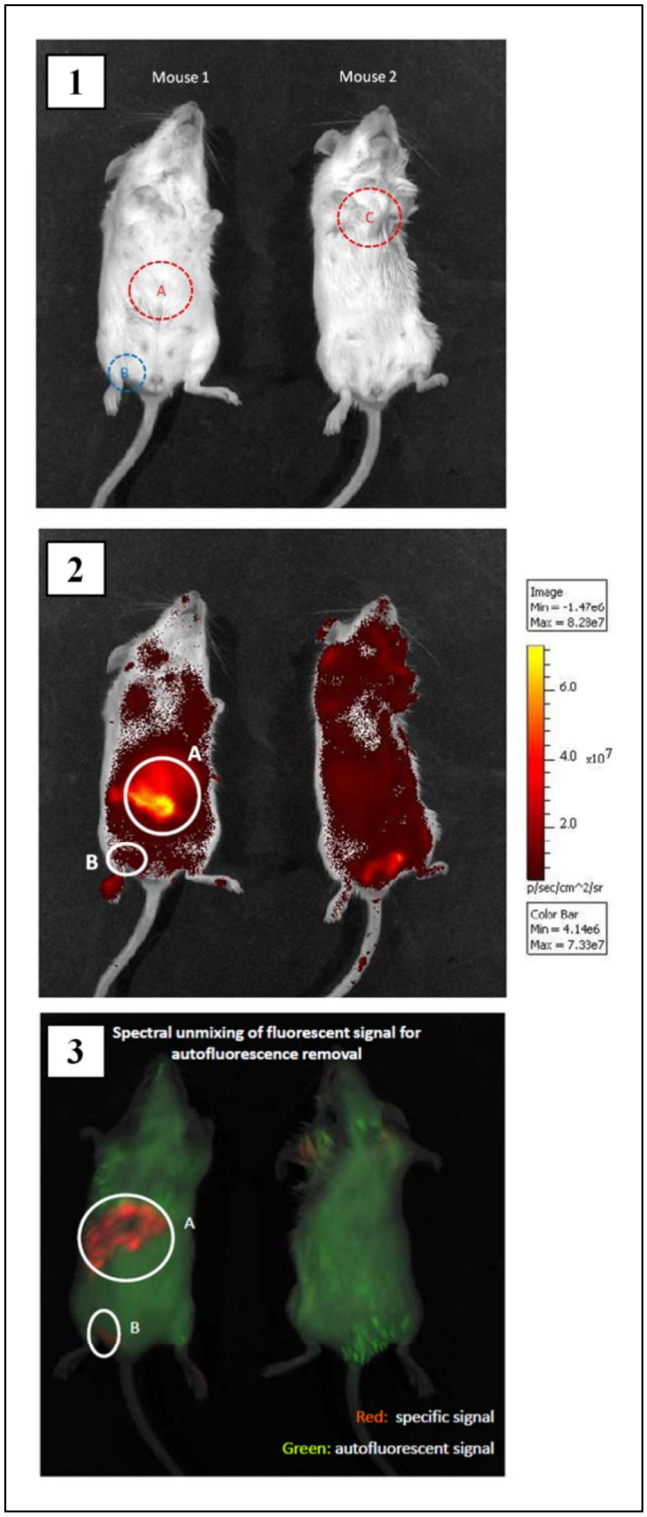

was injected subcutaneously on the ventral surface. Finally, 100 µL MEH-PPV Gd-SPNs (concentration ~ 36 µg/mL) was

Fig. 10 Images of two euthanized mice injected in three locations with (A) 100 µl MEH-PPV Gd-SPNs subcutaneously on the ventral surface, (B) 100 µl MEH-PPV (Gd-SPNs)-IgG intramuscular into the quadricep muscle (~1000x less nanoparticle concentration), and (C) 100 µl MEH-PPV Gd-SPNs deep into the chest cavity. Image (1) is a photograph of the mice in ambient conditions, image (2) is an IVIS image showing the collected fluorescence intensity image against the mice ambient image,

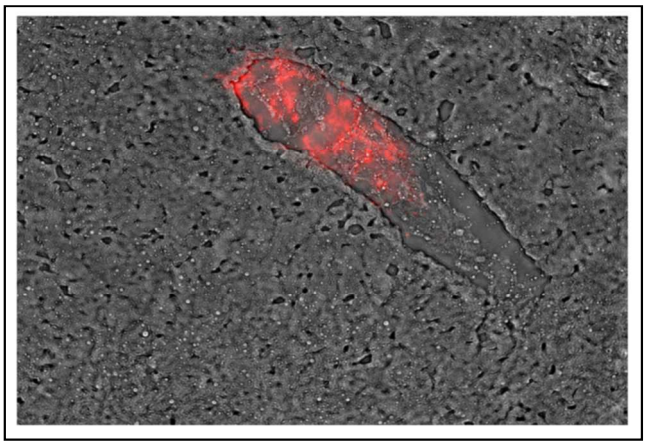

and image (3) is an IVIS processed image that shows the fluorescence from the nanoparticles (red) and the mice's auto-fluorescence (green).

Fig. 11 A bio-image of mouse-spleen tissue after MEH-PPV Gd-SPNs injection into the euthanized mouse's spleen and fixing by snap freezing. The red colour indicates the fluorescence signal from the nanoparticles after tissue auto-fluorescence subtraction.

injected deep into the chest cavity. Fig. 10 shows fluorescence and ambient images of the mice. Considerably high fluorescence brightness was detected from the nanoparticles injected just under the skin (located by (A) in Fig. 10) which suggested that despite the low emission quantum yield, the MEH-PPV nanoparticles could emit through the skin layer and could be distinguished from the mouse's auto-fluorescence. The antibody-conjugated nanoparticles which were injected into the quadricep muscles of the mouse were 1000 times more diluted in terms of nanoparticle concentration, yet could also be detected but with a lower fluorescence intensity ((B) in Fig. 10), which means that the fluorescence could penetrate through several tissue layers. Finally, injecting the nanoparticles deep into the chest cavity resulted in a lost fluorescence signal ((C) in Fig. 10). This is due to the attenuation of the emission as it passed through the animal tissues, with deeper injections resulting in increased attenuation ultimately resulting in the loss of detectable emission. The detectable fluorescence also depended on particle concentration; for a detectable signal from the antibody-conjugated nanoparticles, it was necessary to inject a relatively large amount of conjugated antibodies into a certain area within the mouse's body.

Furthermore, MEH-PPV Gd-SPNs injected into the spleen of a euthanized mouse were successfully imaged after histology. Fig. 11 shows spleen tissue imaged after snap freezing the aseptically removed spleen. Fixing the tissue by placing the whole spleen in 4% formaldehyde destroyed the emission signal but fixing spleen cell suspensions with 1-4% paraformaldehyde did not affect the fluorescence signal. To summarize, two differently emitting Gd-SPNs (MEH-PPV Gd-SPNs; red emitting; with QY ~ 1.5%, and F8BT Gd-SPNs; yellow emitting; QY ~ 33%) were used in an investigation to assess nanoparticle visibility through animal tissue. The nanoparticle fluorescence was distinguishable from the animal auto-fluorescence, however, it was found to be attenuated with injections deeper into the animal tissues. Also, the final concentration of the nanoparticles within the area of interest was found to be pivotal for success of detection within a

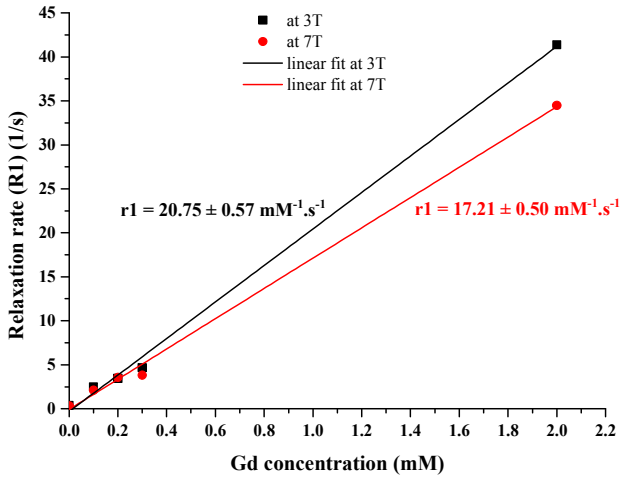

whole animal, with a relatively high concentration needed for a strong

Fig. 12 The relaxation times (R1) versus gadolinium concentration of MEH-PPV Gd-SPNs at 3T and 7T. The relaxivities (r1) are calculated as the slopes of the linear fittings.

Table 2 MRI T_1–weighted relaxation times and their corresponding R1 values measured for different Gd concentrations (i.e. different MEH-PPV Gd-SPNs concentrations), determined using 3T and 7T magnets.

3T			7T		
Gd concentration (mM)	Mean T1 values (s)	R1 values (s^{-1})	Gd concentration (mM)	mean T1 values (s)	R1 values (s^{-1})
water	2.6	0.4	water	2.9	0.3
0.1	0.4	2.5	0.1	0.5	2.1
0.2	0.3	3.5	0.2	0.3	3.6
0.3	0.2	4.7	0.3	0.262	3.82
2	0.02	41.4	2	0.029	34.5

signal. Moreover, preliminary histological tests with MEH-PPV Gd-SPNs revealed that the nanoparticles could be used as tissue-staining materials in such applications.

The concentrations of gadolinium in the purified Gd-SPNs was measured by mass spectrometry and are presented in Table 1. Compared to Gd-QDs prepared with similar lipids (gadolinium concentrations between 0.1 – 0.4 mM)[7], these concentrations were very low (highest being 0.119 mM in the non-concentrated MEH-PPV Gd-SPNs sample). Therefore, the MEH-PPV Gd-SPNs sample was concentrated further to a final gadolinium concentration of 0.3 mM. The relaxation time values (T_1) of this concentration and two successive dilutions (0.2 and 0.1 mM) under two magnetic field strengths (3 Tesla and 7 Tesla) were measured and used to calculate the relaxivity (r_1) of the Gd-SPNs in both fields. The results, reported in Fig. 12 and Table 2, highlight the linear correlation between Gd concentrations and the relaxation rate values (R_1) which are the reciprocals of the T_1 values. The relaxivity (r_1), is calculated for the MEH-PPV Gd-SPNs in Fig. 12 as the slope of the linear relationship, and is determined to be r_1 = 20.75±0.57 $mM^{-1}.s^{-1}$ at 3T, and r_1 = 17.21±0.50 $mM^{-1}.s^{-1}$ at 7T.

Conclusions

Bimodal nanosystems have several advantages over conventional imaging agents in the biological and medical fields. Quantum dots were previously investigated as bimodal MRI-optical imaging agents[7], however, because of the increased concerns about the health and safety issues associated with the use of QDs within living systems (due to their usual toxic compositions), alternative nanoparticles were investigated. In an attempt to provide suitable alternatives, we synthesised four fluorescent organic bimodal nanoparticles that contained gadolinium (Gd-SPNs), with properties such as high fluorescence stability with little to no photo-bleaching after multiple cell image acquisitions or long storage periods.

The Gd-SPNs manufactured in this study had average core diameters around 30 nm with standard deviations of 7 – 22 nm as measured from TEM images, and hydrodynamic diameters around 66 – 128 nm with standard deviations of 27 – 39 nm as measured by NTA. Compared to the bimodal iron oxide/SPNs[25] these Gd-SPNs were significantly smaller and exhibited higher quantum yields. Their MRI T_1–weighted relaxation times were measured revealing a gadolinium concentration dependence with a relaxivity of r_1 = 20.75±0.57 $mM^{-1}.s^{-1}$ at 3T, and r_1 = 17.21±0.50 $mM^{-1}.s^{-1}$ at 7T.

Moreover, the colloidally-stable Gd-SPNs were found to be taken up by live cells and their fluorescence was found to be visible through animal tissue when injected subcutaneously into euthanized mice and a rat pup. The nanoparticle emission signal was dependant on both nanoparticle concentration and injection depth into the tissue.

Acknowledgements

We acknowledge Dr Fiona Winning and Professor Alice Warley, Centre for Ultrastructural Imaging in KCL, for TEM assistance; Mr Andrew Cakebread, Mass Spectrometry Facility in KCL, for Mass Spectrometry; Dr. Baljinder Mankoo, Randall Division of Cell & Molecular Biophysics in KCL, for the kind donation of the HeLa cells; Ms. Agnieszka Siupa, NanoSight NTA Company, for NTA size measurements; Chris Taylor for histopathological assistance and Nicky Walker for conjugation of Gd-SPNs to antibody, DSTL.

We gratefully acknowledge King Abdulaziz University and the Saudi Embassy for funding (ZH).

Notes and references

[a] *Department of Physics, King's College London, Strand, London, WC2R 2LS, UK. * mark.a.green@kcl.ac.uk*

[b] *Division of Imaging Sciences and Biomedical Engineering, King's College London, 4th floor, Lambert Wing, St Thomas' Hospital, London SE1 7EH, UK.*

[c] *Institute of Pharmaceutical Sciences, King's College London, Franklin-Wilkins Building, 150 Stamford Street, London, SE1 9NH, UK.*

[d] *Biomedical Sciences Department, DSTL, Porton Down, Salisbury, SP4 0JQ, UK.*

1. D. Janczewski, Y. Zhang, G. K. Das, D. K. Yi, P. Padmanabhan, K. K. Bhakoo, T. T. Y. Tan and S. T. Selvan, *Microscopy Research and Technique*, 2011, **74**, 563-576.
2. L. E. Jennings and N. J. Long, *Chemical Communications*, 2009, 3511-3524.
3. R. Koole, W. J. M. Mulder, M. M. van Schooneveld, G. J. Strijkers, A. Meijerink and K. Nicolay, *Wiley Interdisciplinary Reviews-Nanomedicine and Nanobiotechnology*, 2009, **1**, 475-491.
4. K. Suhling, P. M. W. French and D. Phillips, *Photochemical & Photobiological Sciences*, 2005, **4**, 13-22.
5. J. A. Levitt, D. R. Matthews, S. M. Ameer-Beg and K. Suhling, *Current Opinion in Biotechnology*, 2009, **20**, 28-36.
6. W. J. M. Mulder, A. W. Griffioen, G. J. Strijkers, D. P. Cormode, K. Nicolay and Z. A. Fayad, *Nanomedicine*, 2007, **2**, 307-324.
7. W. J. M. Mulder, R. Koole, R. J. Brandwijk, G. Storm, P. T. K. Chin, G. J. Strijkers, C. D. Donega, K. Nicolay and A. W. Griffioen, *Nano Letters*, 2006, **6**, 1-6.
8. D. Koktysh, V. Bright and W. Pham, *Nanotechnology*, 2011, **22**.
9. V. Holzapfel, M. Lorenz, C. K. Weiss, H. Schrezenmeier, K. Landfester and V. Mailander, *Journal of Physics-Condensed Matter*, 2006, **18**, S2581-S2594.
10. F. Wang, X. L. Chen, Z. X. Zhao, S. H. Tang, X. Q. Huang, C. H. Lin, C. B. Cai and N. F. Zheng, *Journal of Materials Chemistry*, 2011, **21**, 11244-11252.
11. G. A. F. van Tilborg, E. Vucic, G. J. Strijkers, D. P. Cormode, V. Mani, T. Skajaa, C. P. M. Reutelingsperger, Z. A. Fayad, W. J. M. Mulder and K. Nicolay, *Bioconjugate Chemistry*, 2010, **21**, 1794-1803.
12. G. Liu, H. X. Wu, H. R. Zheng, L. H. Tang, H. Hu, H. Yang and S. P. Yang, *Journal of Materials Science*, 2011, **46**, 5959-5968.
13. Y. L. Liu, K. L. Ai, Q. H. Yuan and L. H. Lu, *Biomaterials*, 2011, **32**, 1185-1192.
14. K. Wang, J. Ruan, Q. R. Qian, H. Song, C. C. Bao, X. Q. Zhang, Y. F. Kong, C. L. Zhang, G. H. Hu, J. Ni and D. X. Cui, *Journal of Nanobiotechnology*, 2011, **9**.
15. S. A. Corr, Y. P. Rakovich and Y. K. Gun'ko, *Nanoscale Research Letters*, 2008, **3**, 87-104.
16. G. A. F. van Tilborg, W. J. M. Mulder, N. Deckers, G. Storm, C. P. M. Reutelingsperger, G. J. Strijkers and K. Nicolay, *Bioconjugate Chemistry*, 2006, **17**, 741-749.
17. C. Medina, M. J. Santos-Martinez, A. Radomski, O. I. Corrigan and M. W. Radomski, *British Journal of Pharmacology*, 2007, **150**, 552-558.
18. Z. Hashim, P. Howes and M. Green, *Journal of Materials Chemistry*, 2011, **21**, 1797-1803.
19. P. Howes, M. Green, J. Levitt, K. Suhling and M. Hughes, *Journal of the American Chemical Society*, 2010, **132**, 3989-3996.
20. N. A. A. Rahim, W. McDaniel, K. Bardon, S. Srinivasan, V. Vickerman, P. T. C. So and J. H. Moon, *Adv. Mater.*, 2009, **21**, 3492.
21. C. Wu, B. Bull, C. Szymanski, K. Christensen and J. McNeill, *ACS Nano*, 2008, **2**, 2415-2423.
22. J. H. Moon, P. MacLean, W. McDaniel and L. F. Hancock, *Chemical Communications*, 2007, 4910-4912.
23. A. Vaidya, Y. G. Sun, Y. Feng, L. Emerson, E. K. Jeong and Z. R. Lu, *Pharm. Res.*, 2008, **25**, 2002-2011.

24. Q. Xu, L. Liu, L. Zhu, M. Yu, Q. Yang and S. Wang, *Frontiers of Chemistry in China*, 2010, **5**, 166-170.
25. P. Howes, M. Green, A. Bowers, D. Parker, G. Varma, M. Kallumadil, M. Hughes, A. Warley, A. Brain and R. Botnar, *Journal of the American Chemical Society*, 2010, **132**, 9833-9842.
26. D. Magde, G. E. Rojas and P. G. Seybold, *Photochemistry and Photobiology*, 1999, **70**, 737-744.
27. Atto 390 data sheet http://www.atto-tec.com/fileadmin/user_upload/Katalog_Flyer_Support/ATTO_390.pdf, Accessed 22 November 2011, 2011.
28. A. Sillen and Y. Engelborghs, *Photochemistry and Photobiology*, 1998, **67**, 475-486.
29. E. Fiserova and M. Kubala, *Journal of Luminescence*, 2012, **132**, 2059-2064.
30. A. Protti, A. Sirker, A. M. Shah and R. Botnar, *Journal of Magnetic Resonance Imaging*, 2010, **32**, 878-886.
31. M. R. Makowski, A. J. Wiethoff, U. Blume, F. Cuello, A. Warley, C. H. P. Jansen, E. Nagel, R. Razavi, D. C. Onthank, R. R. Cesati, M. S. Marber, T. Schaeffter, A. Smith, S. P. Robinson and R. M. Botnar, *Nature Medicine*, 2011, **17**, 383-388.
32. S. Kumari, M. G. Swetha and S. Mayor, *Cell Research*, 2010, **20**, 256-275.
33. E. Mahon, A. Salvati, F. Baldelli Bombelli, I. Lynch and K. A. Dawson, *J Control Release*, 2012.
34. N. Hao, L. Li, Q. Zhang, X. Huang, X. Meng, Y. Zhang, D. Chen, F. Tang, L, Li, *Microporous and Mesoporous Materials*, 2012, **162**, 14-23.
35. J. Contreras, J, Xie, Y. J. Chen, H. Pei, G. Zhang, C. L. Fraser, S. F. Hamm-Alvarez, *ACS Nano*. 2010, **4**, 2735–2747.
36. A. Aderem and D. M. Underhill, *Annual Review of Immunology*, 1999, **17**, 593-623.
37. R. A. Khanbeigi, A. Kumar, F. Sadouki, C. Lorenz, B. Forbes, L. A. Dailey and H. Collins, *Journal of Controlled Release*, 2012, **162**, 259-266.
38. L. A. Dailey, E. Kleemann, T. Merdan, H. Petersen, T. Schmehl, T. Gessler, J. Hanze, W. Seeger and T. Kissel, *Journal of Controlled Release*, 2004, **100**, 425-436.
39. E. Chang, W. W. Yu, V. L. Colvin and R. Drezek, *Journal of Biomedical Nanotechnology*, 2005, **1**, 397-401.
40. E. L. Bentzen, I. D. Tomlinson, J. Mason, P. Gresch, M. R. Warnement, D. Wright, E. Sanders-Bush, R. Blakely and S. J. Rosenthal, *Bioconjugate Chemistry*, 2005, **16**, 1488-1494.
41. M. Y. Berezin and S. Achilefu, *Chem. Rev.*, 2010, **110**, 2641-2684.
42. H. R. Zhang, X. F. Lu, Y. Li, X. C. Ai, X. K. Zhang and G. Q. Yang, *Journal of Photochemistry and Photobiology a-Chemistry*, 2002, **147**, 15-23.
43. B. J. Bain and R. Gupta, *A - Z of Haematology*, Blackwell Publishing Ltd, Oxford, 2003.